

Saima Noreen*, Ali J. Chamkha and Aqsa Jahan

Analysis of Williamson fluid flow incorporating Darcy's resistance and electro kinetics: analytical and numerical results

<https://doi.org/10.1515/zna-2023-0052>

Received March 2, 2023; accepted May 22, 2023;

published online June 13, 2023

Abstract: This article discusses a mathematical model for the electrokinetic and Darcy's resistance of Williamson fluid in an electroosmotic pumping environment. The zeta potential at walls aids in peristaltic movement, and porous dissipation is incorporated into this modulation by the Williamson fluid's material parameters. Through the use of Debye-Huckel approximations, long wavelengths, and low Reynolds numbers, the model equations are simplified. Mathematica software is used to produce analytical and numerical results, and plots and analyses are done using the included parameters on physical quantities of interest. This study has various practical applications, such as modifying belt resistance in laboratory drainage testing and improving pipeline design. It could also potentially aid in the development of blood filtration and purification techniques and optimize drug delivery systems that utilize fluids. It is observed that the modified Darcy's law is more accurate for porosity effects in electroosmotic peristaltic channels and results in higher shear stress at the channel wall compared to Darcy's law.

Keywords: analytical solutions; electroosmosis; modified Darcy's law; numerical solutions; peristalsis

Nomenclature

$d^*, d1^* d2^*$	dimensional channel width [L]
U_{HS}	Helmholtz-Smoluchowski velocity [LT^{-1}]
$d, d1, d2$	non-dimensional channel width [–]
λ_D	debye length [L]

a^*, b^*	dimensional wave amplitude [L]
λ	wave length [L]
a, b	dimensionless wave amplitude [–]
μ_o	zero shear rate viscosity [$ML^{-1}T^{-1}$]
p^*	dimensional pressure [MLT^{-2}]
β	mobility of the medium C
ρ	dimensionless pressure [–]
Γ	time constant [T]
f^*, g^*	dimensional velocity component [LT^{-1}]
ρ_e	net charge density [ML^{-3}]
f, g	non-dimensional velocity component [–]
E	electric field [$MT^{-3}A^{-1}$]
ρ	fluid density [ML^{-3}]
ϵ	permittivity of medium [–]
W	Weissenberg number [–]
ϵ	permittivity of free space [$T^4A^2M^{-1}L^{-3}$]
Re	Reynold number [–]
Da	Darcy number [–]
δ	wave number [–]
F	flow rate [L^3T^{-1}]
c	wave speed [LT^{-1}]
φ^*	dimensional electric potential distribution [$ML^2T^{-2}I^{-1}$]
ξ^*, η^*	dimensional rectangular coordinates [L]
φ	non-dimensional electric potential distribution [–]
ξ, η	non-dimensional rectangular coordinates [–]
ϕ	phase difference [L]
$h1^*, h2^*$	dimensional walls of the channel [L]
Ψ	stream function [L^2T^{-1}]
$h1, h2$	non-dimensional walls of the channel [–]
τ^*	cauchy stress tensor [$ML^{-1}T^{-1}$]
K_B	Boltzmann constant [$ML^2T^{-2}K^{-1}$]
k	porosity parameter [L^2]
m	electroosmotic parameter [–]
μ_∞	infinite shear rate viscosity [L^2]
t^*	dimensional time [T]
γ^*	dimensional stain rate [T^{-1}]
t	non-dimensional time [–]
γ	non-dimensional strain rate [–]

1 Introduction

Porous media are known to enhance the liquid-to-solid contact surface. This has been the focus of academic research for a number of decades, specifically in the area of fluid passage through porous media. When a pressure differential is applied, porous materials facilitate the transport of fluids through interconnected spaces or pores. In applications

*Corresponding author: Saima Noreen, Department of Mathematics, COMSATS University Islamabad, Park road Tarlai kalan, Islamabad 45550, Pakistan, E-mail: laurel_lichen@yahoo.com

Ali J. Chamkha, Kuwait College of Science & Technology, 7th Ring Road, Doha District, 3500, Kuwait City, Kuwait

Aqsa Jahan, Department of Mathematics, COMSATS University Islamabad, Park road Tarlai kalan, Islamabad 45550, Pakistan

such as geophysics, chemical reactors, petroleum industries, nuclear reactors, hydrogeology, and environmental studies, the ability to convey substances through a porous medium is crucial.

Darcy suggested linking solid and liquid phases through a porous medium in 1885. Many porous medium researchers interested in organic and dynamic pores study his law. Darcy's law applies exclusively to laminar flow at low Reynolds numbers. Focusing on minor potential gradients, Childs and Tzimas [1], Whitaker [2], and Hubbert [3] have provided theoretical derivations and practical implementations of Darcy's law in porous media for the flow of underground fluids. Starov et al. [4] investigated the effect of permeability on fluid flow in porous media, whereas Graham et al. [5] investigated the effect of non-zero inertial forces on compressible Newtonian fluid flow in porous materials. Their investigation also included an analysis of how variations in the magnitude of the inertial forces and the geometry of the medium impact the flow characteristics. Hayat et al. [6] investigated the impact of slip conditions on peristaltic viscous fluid flow in porous media. Ramesh et al. [7] studied peristaltic flow through an inclined, asymmetric channel in a porous medium.

Darcy's Law is straightforward and simple to employ. It provides a simple mathematical model for predicting fluid flow in porous media and can be used as a benchmark for evaluating more complex models that may include fluid characteristics, gravity, nonlinear thermal radiation, activation energy, Hall current and heterogeneity [8–11].

Darcy's Law has limitations due to the homogeneity and isotropy assumptions. In addition, it is only applicable under particular conditions, such as steady-state flow and low Reynolds numbers.

Although Darcy's law was frequently employed in non-Newtonian fluid flow, the full details for porous media can be properly introduced by looking at modified Darcy's law. Darcy's law fails to account for the effect of surface tension on fluid in a porous medium, and it is impossible to disregard the significance of resistance in non-Newtonian fluxes. To address these concerns, modified variants of Darcy's law have been proposed, such as the modification presented by Gisinger et al. [12], which was demonstrated by large eddy simulations. Vasudev et al. [13] investigated Williamson peristaltic fluid flow through porous media and heat transfer, Khan et al. [14] studied micropolar fluids, and Imomnazarov et al. [15] investigated conducting fluids using modified versions of Darcy's law. Recent research on these topics is available in references [16–19].

Fluids flowing through porous materials experience varying force and energy due to material expansion and

contraction, causing non-linear flow speed, especially at high speeds, known as non-Darcy flow. This phenomenon is significant in the oil industry when fluid must traverse porous rocks with high inflow and outflow. Forcheimer [20] developed a non-Darcy formula for the Darcy equation to incorporate this phenomenon. Studies [21, 22] have investigated various aspects of non-Darcy porous media, such as electroosmotic transport, peristaltic motion, and the flow of nanofluids.

Electroosmosis is the movement of a liquid through a porous material due to the presence of an electric field. Electro-osmosis plays a crucial role in various practical applications at different length scales, including geological, geotechnical, biomechanical, gas and oil industry, and lab sciences. It is also used to remove heavy metal ions from soil and solidify soft clay to prevent land collapse. Several studies investigated electro-osmosis in porous media, including Gupta et al. [23] and Chen et al. [24] who studied its behavior in non-Newtonian fluids. Bowen et al. [25] investigated the zeta potential of membranes using electro-osmosis, while Gravesen et al. [26] used flow theory to explain fluid behavior in microfabrication technology. Studies by Dennis et al. [27] and Chiang et al. [28] focused on the flow of incompressible fluids in symmetric channels, while Hawa et al. [29] analyzed steady flow models approaching a significant Reynolds number. Latham [30] discovered the occurrence of peristalsis in channels. Elshehawey et al. [31] have studied the transport of viscous fluids through asymmetric channels in porous media. Numerous researchers have contributed to the study of peristaltic flow under different effects and boundary conditions. Hayat et al. [6] analyzed slip effects using the Adomian decomposition method, while Machireddy et al. [32] investigated the effects of joule heating and velocity slip on MHD peristaltic flow. Furthermore, relevant investigations are documented in [33–39].

Hydrogels, lubricating oils, and blood have difficult rheology because their strain rate is not proportional to their shear stress. These fluids are employed in ethyl alcohol and gibberellic acid production, microbiological and gasification fermentation, and crude oil extraction from petroleum fuels. In addition, food processing, metallurgy, drilling, and biotechnology use it. Thus, several studies have investigated non-Newtonian fluid flow problems. Recent researches [40, 41] investigate the use of non-Newtonian fluids for drug delivery and improved therapeutic approaches in hemodynamics. Williamson experimentally tested his fluid model in 1929. The investigations [42–45] investigate the behavior of Williamson fluid in various geometries, including straight channel and wedge-geometry, and under the influence of

non-linear thermal radiation, heat transfer, and magnetic field, with a particular emphasis on unsteady flow and variable thermal conductivity.

Current study aims to investigate the effects of modified Darcy's resistance and electrokinetics on the Williamson fluid flow in a planar symmetric channel with electrochemical walls. Both analytical and numerical methods are employed, with the former being based on the regular perturbation method, and the latter utilizing the NDSolve command in Mathematica 11. The numerical solutions are compared with analytical solutions to enhance the analysis. Our research is novel in that it combines the considerations of Darcy's resistance and electrokinetics in analyzing the behavior of Williamson fluid flow in porous media, offering new insights into this type of fluid's properties. For fluid flow through channels subject to electric fields, such as electroosmotic flow, electrophoresis, and electrokinetic pumping, the modified Darcy law provides a predictive framework for microfluidics and electrochemistry.

2 Mathematical formulation

2.1 Geometry of the flow problem

Consider electroosmotic peristaltic flow via porous medium in a symmetric channel with rectangular coordinate system (ξ^*, η^*) and velocity field $(f^*, g^*, 0)$. The geometry of the channel is presented in Figure 1. The wave propagates along the length of the channel i.e., ξ direction. This flow is produced by a sinusoidal wave propagating at a constant speed c along the channel walls. The channel walls are flexible with channel width $2d$. The electric field E is supposed to be applied axially on the fluid flow.

Mathematically, Symmetric channel geometry is represented as by (1):

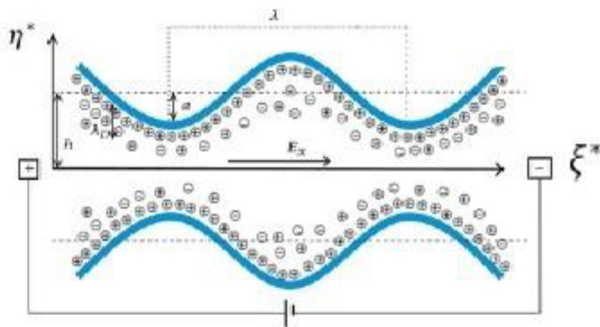


Figure 1: Geometry of flow problem.

$$\eta^* = \pm h^*(\xi^*, t^*) = \pm \left[d^* + a^* \sin \frac{2\pi}{\lambda} (\xi^* - ct^*) \right], \quad (1)$$

where a^* is the amplitude of wave, λ is the wavelength, c is wave speed, d^* is the width of the channel and the displacement of the walls of channel is denoted by $\pm h^*$ respectively.

2.2 Fluid model

Cauchy stress tensor for Williamson fluid Eq. (2–12) is defined as:

$$\tau^* = -p^*I + S^*, \quad (2)$$

where S^* is extra stress tensor defined as

$$S^* = \left(\mu_\infty + \frac{\mu_0 + \mu_\infty}{(1 - \Gamma\dot{\gamma}^*)} \right) A^*, \quad (3)$$

Strain rate is written as:

$$\begin{aligned} \dot{\gamma}^* &= \sqrt{\frac{1}{2} \text{trace} A^2} \\ &= \sqrt{\left(\frac{\partial f^*}{\partial \xi^*} \right)^2 + \left(\frac{\partial f^*}{\partial \eta^*} + \frac{\partial g^*}{\partial \xi^*} \right)^2 + 2 \left(\frac{\partial g^*}{\partial \eta^*} \right)^2}, \end{aligned} \quad (4)$$

where μ_0 and μ_∞ are zero and infinite shear rate respectively. A^* is Rivlin Ericksen tensor given by:

$$A^* = (\nabla V) + (\nabla V)^T,$$

$$\text{where } \mathbf{V} = [f^*(\xi^*, \eta^*, t^*), g^*(\xi^*, \eta^*, t^*), 0] \quad (5)$$

In this study, $\mu_\infty = 0$ and $\Gamma\dot{\gamma}^* < 1$, S^* is written as,

$$S^* = \mu_0(1 + \Gamma\dot{\gamma}^*)A^* \quad (6)$$

The component form:

$$S_{\xi^*\xi^*}^* = 2\mu_0(1 + \Gamma\dot{\gamma}^*) \frac{\partial f^*}{\partial \xi^*} \quad (7)$$

$$S_{\xi^*\eta^*}^* = \mu_0(1 + \Gamma\dot{\gamma}^*) \left(\frac{\partial f^*}{\partial \eta^*} + \frac{\partial g^*}{\partial \xi^*} \right) \quad (8)$$

$$S_{\eta^*\eta^*}^* = 2\mu_0(1 + \Gamma\dot{\gamma}^*) \frac{\partial g^*}{\partial \eta^*} \quad (9)$$

The law governing Darcy resistance [17] is

$$R = -\frac{\mu_0}{k} (1 + \Gamma\dot{\gamma}^*) \mathbf{V}^* \quad (10)$$

The component form:

$$R_\xi = -\frac{\mu_0}{k} (1 + \Gamma\dot{\gamma}^*) f^* \quad (11)$$

$$R_\eta = -\frac{\mu_0}{k} (1 + \Gamma\dot{\gamma}^*) g^* \quad (12)$$

here in the above equations f^* and g^* are the respective velocity components in ξ^* and η^* direction, Γ is time constant and k is permeability of porous medium.

2.3 Potential distribution

By using Gauss law, the Poisson equation is defined as:

$$\nabla^2 \varphi^* = -\frac{\rho_e}{\epsilon_0 \epsilon}. \quad (13)$$

where φ^* , ρ_e , ϵ_0 and ϵ indicates electric potential, total charge density, permittivity of free space and dielectric permittivity respectively.

The net charge density ρ_e follows the Boltzmann distribution, which is given by

$$\rho_e = -z_v e (n^{*-} - n^{*+}), \quad (14)$$

here the negative (n^{*-}) and positive (n^{*+}) ions are defined through ρ_e of the Boltzmann Eq:

$$n^{*\pm} = n_0^* e^{\left(\pm \frac{e z_v}{T_{av} K_B} \varphi^*\right)}, \quad (15)$$

where e is the electronic charge, n_0 is the average number of anions and cations, K_B is the Boltzmann constant, z_v is the ions valence and T_{av} is the average temperature.

Nernst Planck equation employed to investigate the number of charge density and potential distribution defined as:

$$\begin{aligned} & \left(\frac{\partial n_{\pm}^*}{\partial t^*} + f \frac{\partial n_{\pm}^*}{\partial \xi^*} + g \frac{\partial n_{\pm}^*}{\partial \eta^*} \right) \\ & = D_{\pm} \left(\frac{\partial^2 n_{\pm}^*}{\partial \xi^{2*}} + g \frac{\partial^2 n_{\pm}^*}{\partial \eta^{2*}} \right) \pm \frac{D_{\pm} e z_v}{T_{av} K_B} \left(\frac{\partial}{\partial \xi^*} \left(n_{\pm}^* \frac{\partial \varphi^*}{\partial \xi^*} \right) \right. \\ & \left. + \frac{\partial}{\partial \eta^*} \left(n_{\pm}^* \frac{\partial \varphi^*}{\partial \eta^*} \right) \right), \end{aligned} \quad (16)$$

where D_{\pm} is diffusivity of ionic species.

Now introduce dimensionless variables,

$$\xi = \frac{\xi^*}{\lambda}, \quad \eta = \frac{\eta^*}{d}, \quad t = \frac{c t^*}{\lambda}, \quad f = \frac{f^*}{c}, \quad g = \frac{\lambda g^*}{c d},$$

$$\varphi = \frac{e z_v}{T_{av} K_B} \varphi^*, \quad m = \frac{d}{\lambda_D}, \quad n = \frac{n^*}{n_0},$$

$$\lambda_D = \frac{1}{e z_v} \sqrt{\frac{T_{av} \epsilon_0 \epsilon K_B}{2 n_0}}, \quad U_{hs} = -\frac{E T_{av} \epsilon_0 \epsilon K_B}{\mu e z_v}, \quad \delta = \frac{d}{\lambda},$$

$$\beta = \frac{U_{hs}}{c}, \quad P_e = \frac{c \lambda}{D_{\pm}}.$$

Here, ξ is the non-dimensional axial coordinate, η is the non-dimensional transverse coordinate, m is electroosmotic parameter, c is the wave speed, φ is non-dimensional electric potential, t is non-dimensional time, λ_D is Debye length, λ is wavelength, δ is wave number, U_{hs} is Helmholtz-Smoluchowski velocity, P_e is ionic Peclet number, β is the mobility of the medium.

After non-dimensionalization and under long-wavelength assumption, equation (16) is termed as,

$$0 = \frac{\partial^2 n_{\pm}}{\partial \eta^2} + \frac{\partial}{\partial \eta} \left(n_{\pm} \frac{\partial \varphi}{\partial \eta} \right), \quad (17)$$

Equation (17) subjected to boundary conditions $n_{\pm}(\varphi = 0) = 1$, $\frac{\partial n_{\pm}}{\partial y} \left(\frac{\partial \varphi}{\partial y} = 0 \right) = 0$, we obtained as:

$$n_{\pm} = e^{\mp \varphi} \quad (18)$$

By using equations (18) and (14), equation (13) takes the form:

$$\frac{\partial^2 \varphi}{\partial y^2} = m^2 \sinh \varphi \quad (19)$$

Employing Debye-Hückel linearization approximation i.e., $\sinh \varphi \approx \varphi$. Then, Eq. (19) becomes

$$\frac{d^2 \varphi}{d\eta^2} = m^2 \varphi. \quad (20)$$

The analytical solution by utilizing Eqs. (13–20) subject to boundary conditions (21) gives Eq. (22).

$$\frac{\partial \varphi}{\partial \eta}(0), \quad \varphi(h) = 1, \quad (21)$$

is obtained as;

$$\Phi(\eta) = \frac{\cosh(m\eta)}{\cosh(mh)} \quad (22)$$

2.4 Governing equations

Flow equations such as law of conservation of mass (23) and equation of motion (24, 25) for incompressible 2D flow under electric field and modified Darcy's law are, in component form.

$$\frac{\partial f^*}{\partial \xi^*} + \frac{\partial g^*}{\partial \eta^*} = 0, \quad (23)$$

$$\begin{aligned} & \rho \left(\frac{\partial}{\partial t^*} + f^* \frac{\partial}{\partial \xi^*} + g^* \frac{\partial}{\partial \eta^*} \right) f^* \\ & = -\frac{\partial P^*}{\partial \xi^*} + \left(\frac{\partial S_{\xi^* \xi^*}^*}{\partial \xi^*} + \frac{\partial S_{\xi^* \eta^*}^*}{\partial \eta^*} \right) + \rho_e E \\ & \quad - \frac{\mu_0}{k} (1 + \Gamma \gamma^*) f^*, \end{aligned} \quad (24)$$

$$\begin{aligned} & \rho \left(\frac{\partial}{\partial t^*} + f^* \frac{\partial}{\partial \xi^*} + g^* \frac{\partial}{\partial \eta^*} \right) g^* \\ & = -\frac{\partial P^*}{\partial \eta^*} + \left(\frac{\partial S_{\xi^* \eta^*}^*}{\partial \xi^*} + \frac{\partial S_{\eta^* \eta^*}^*}{\partial \eta^*} \right) - \frac{\mu_0}{k} (1 + \Gamma \gamma^*) g^*, \end{aligned} \quad (25)$$

here P^* is the fluid pressure, ρ is the density of the fluid, E is applied electric field, ρ_e is electric charge density, t^* is the time.

2.5 Non-dimensionalization

Now introducing the non-dimensional variables (26) and stream function (27) by

$$\begin{aligned}\xi &= \frac{\xi^*}{\lambda}, \quad \eta = \frac{\eta^*}{d}, \quad t = \frac{ct^*}{\lambda}, \quad f = \frac{f^*}{c}, \quad g = \frac{\lambda g^*}{cd}, \\ p &= \frac{d^2}{\lambda c \mu} p^*, \quad m = \frac{d}{\lambda_D}, \quad \beta = \frac{U_{hs}}{c}, \\ \lambda_D &= \frac{1}{e z_v} \sqrt{\frac{T_{av} \epsilon_0 \in K_B}{2n_0}}, \quad U_{hs} = -\frac{ET_{av} \epsilon_0 \in K_B}{\mu e z_v}, \\ S_{ij} &= \frac{d}{c \mu} S_{ij}^* (i, j = 1, 2, 3 \dots), \\ \psi^* &= \frac{\psi}{cd}, \quad h = \frac{h^*}{d}, \quad \delta = \frac{d}{\lambda}, \quad R_e = \frac{\rho cd}{\mu}, \quad Da = \frac{k}{d^2}, \\ W &= \frac{\Gamma c}{d}, \quad \dot{\gamma} = \dot{\gamma}^* \frac{d}{c}.\end{aligned}\quad (26)$$

here, p is non-dimensional pressure, W is Weissenberg number, U_{hs} is Helmholtz-Smoluchowski velocity, ψ is non-dimensional stream function, R_e is Reynolds number, Da is Darcy number.

Now introducing stream function ψ as:

$$f = \frac{\partial \psi}{\partial \eta}, \quad g = -\frac{\partial \psi}{\partial \xi}.\quad (27)$$

The Eq. (23) is identically satisfied and from Eqs. (24)–(25), subject to long-wavelength assumption, we get:

$$\begin{aligned}\frac{\partial p}{\partial \xi} &= \frac{\partial}{\partial \eta} \left[\frac{\partial^2 \psi}{\partial \eta^2} + W \left(\frac{\partial^2 \psi}{\partial \eta^2} \right)^2 \right] + m_e^2 \beta \varphi \\ &\quad - \frac{1}{Da} \left[\frac{\partial \psi}{\partial \eta} + W \left(\frac{\partial^2 \psi}{\partial \eta^2} \right) \left(\frac{\partial \psi}{\partial \eta} \right) \right],\end{aligned}\quad (28)$$

$$\frac{\partial p}{\partial \eta} = 0,\quad (29)$$

Eliminating pressure from Eq. (28) and Eq. (29), we get

$$\begin{aligned}\frac{\partial^2}{\partial \eta^2} \left[\frac{\partial^2 \psi}{\partial \eta^2} + 2W \left(\frac{\partial^2 \psi}{\partial \eta^2} \right)^2 \right] + m_e^2 \beta \frac{\partial \varphi}{\partial \eta} \\ - \frac{1}{Da} \left[\frac{\partial^2 \psi}{\partial \eta^2} + W \left(\left(\frac{\partial^2 \psi}{\partial \eta^2} \right)^2 + \left(\frac{\partial \psi}{\partial \eta} \right) \left(\frac{\partial^3 \psi}{\partial \eta^3} \right) \right) \right] = 0.\end{aligned}\quad (30)$$

Eq. (30) subject to the boundary conditions 31(a,b) are:

$$\frac{d^2 \psi}{d\eta^2} = 0, \quad \psi = 0, \quad \text{at } \eta = 0,\quad (31a)$$

$$\frac{\partial \psi}{\partial \eta} = 0, \quad \psi = F, \quad \text{at } \eta = h(\xi) = 1 + a \sin 2\pi(\xi - t),\quad (31b)$$

Moreover, non-dimensional time dependent flow rate defined as:

$$F = Ce^{-Dt},\quad (32)$$

here C and D are constants, the flow rate valued based on C . If the flow rate is negative, it suggests retrograde pumping, if the $C > 0$ flow rate is positive, it represents peristaltic flow of fluid.

3 Solution

Numerical solutions (Table 4) are computed for comparison with analytical solutions. The analytical solutions of the following systems are obtained by using perturbation technique. Therefore, we expand ψ , $dp/d\xi$ and F (33–41) about fluid parameter W as:

$$\psi = \psi_0 + W\psi_1 + O(W)^2,\quad (33)$$

$$\frac{dp}{d\xi} = \frac{dp_0}{d\xi} + W \frac{dp_1}{d\xi} + O(W)^2,\quad (34)$$

$$F = F_0 + WF_1 + O(W)^2,\quad (35)$$

3.1 Zeroth order system $O(W)^0$

$$\frac{\partial^4 \psi_0}{\partial \eta^4} + m^2 \beta \frac{\partial \varphi}{\partial \eta} - \frac{1}{Da} \left[\frac{\partial^2 \psi_0}{\partial \eta^2} \right] = 0,\quad (36)$$

$$\frac{dp_0}{d\xi} = \frac{\partial^3 \psi_0}{\partial \eta^3} + m^2 \beta \varphi - \frac{1}{Da} \left[\frac{\partial \psi_0}{\partial \eta} \right],\quad (37)$$

Subject to boundary conditions

$$\frac{d^2 \psi_0}{d\eta^2} = 0, \quad \psi_0 = 0, \quad \text{at } \eta = 0,\quad (38a)$$

$$\frac{\partial \psi_0}{\partial \eta} = 0, \quad \psi_0 = F_0, \quad \text{at } \eta = h(\xi) = 1 + a \sin 2\pi(\xi - t),\quad (38b)$$

3.2 First order system $O(W)^1$

$$\begin{aligned}\frac{\partial^4 \psi_1}{\partial \eta^4} + 2 \left(\frac{\partial^2 \psi_0}{\partial \eta^2} \right) \left(\frac{\partial^4 \psi_0}{\partial \eta^4} \right) + 2 \left(\frac{\partial^3 \psi_0}{\partial \eta^3} \right)^2 \\ - \frac{1}{Da} \left[\frac{\partial^2 \psi_1}{\partial \eta^2} + \left(\frac{\partial^2 \psi_0}{\partial \eta^2} \right)^2 + \left(\frac{\partial \psi_0}{\partial \eta} \right) \left(\frac{\partial^3 \psi_0}{\partial \eta^3} \right) \right] = 0,\end{aligned}\quad (39)$$

$$\begin{aligned}\frac{dp_1}{d\xi} = \frac{\partial^3 \psi_1}{\partial \eta^3} + 2 \left(\frac{\partial^2 \psi_0}{\partial \eta^2} \right) \left(\frac{\partial^3 \psi_0}{\partial \eta^3} \right) \\ - \frac{1}{Da} \left[\frac{\partial \psi_1}{\partial \eta} + \left(\frac{\partial \psi_0}{\partial \eta} \right) \left(\frac{\partial^2 \psi_0}{\partial \eta^2} \right) \right],\end{aligned}\quad (40)$$

Subject to boundary conditions

$$\frac{d^2\psi_1}{d\eta^2} = 0, \psi_1 = 0, \text{ at } \eta = 0, \quad (41a)$$

$$\frac{\partial\psi_1}{\partial\eta} = 0, \psi_1 = F_1, \text{ at } \eta = h(\xi) = 1 + a \sin 2\pi(\xi - t), \quad (41b)$$

3.3 Solution expressions

Flow chart for numerical scheme and analytical closed forms of solutions (42–43) are presented in Appendix.

4 Computational results and discussion

This section presents the results of electro-osmotically assisted peristaltic transport of a Williamson fluid through a symmetric channel in the presence of modified Darcy's porosity. In Figures 2–7, the effects of several factors such as

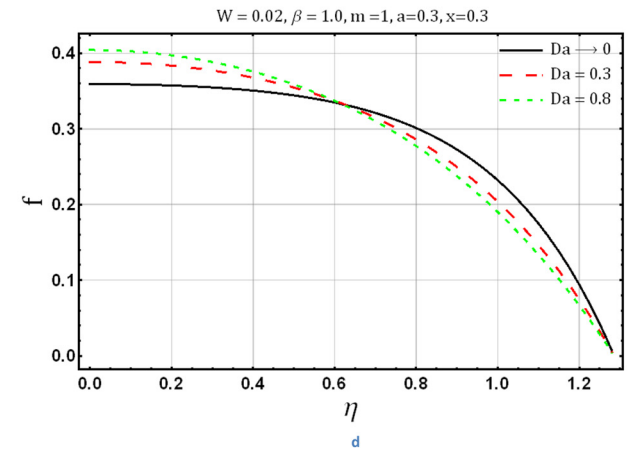
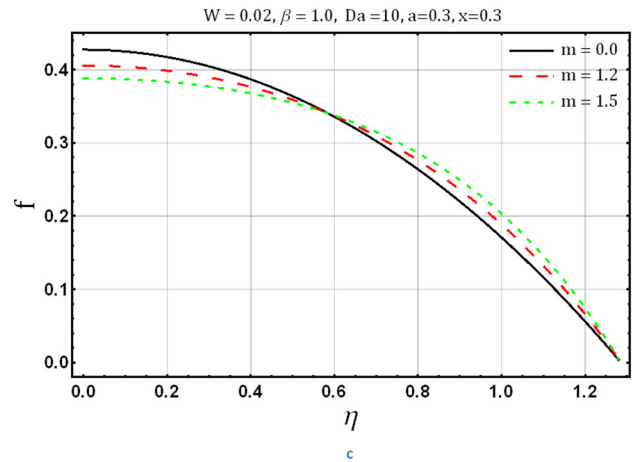
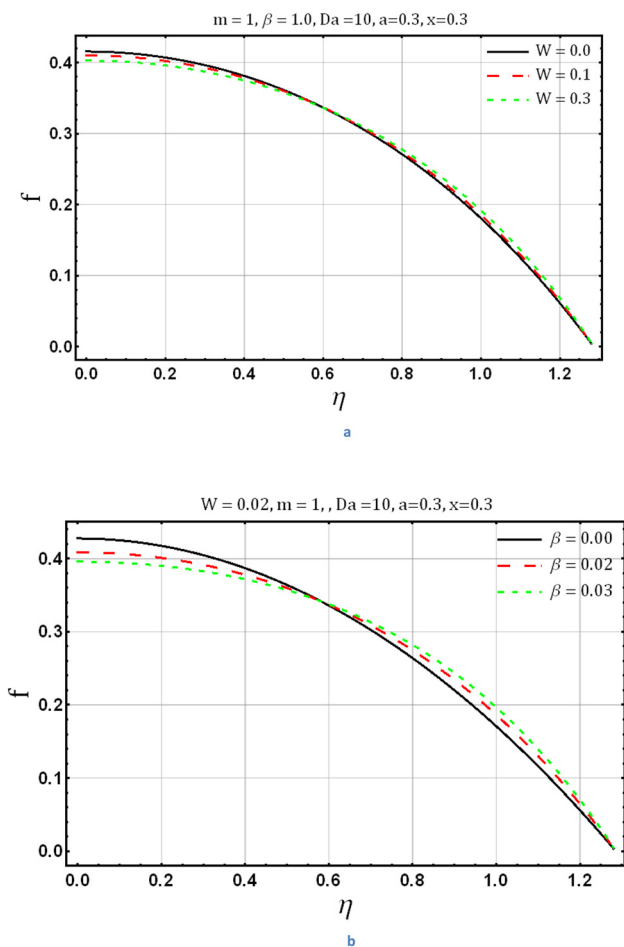


Figure 2: (continued)

Weissenberg W , Darcy number Da , electroosmotic parameter m , and medium mobility β on velocity f , pressure gradient $dp/d\xi$ and trapping are shown. Tables (1–3) have been created to compare analytical and numerical solutions. Analytical solutions were obtained using the perturbation method, while numerical solutions were obtained using the MATHEMATICA software.

4.1 Flow characteristics

In Figure 2(a–d), the influential factors, Weissenberg number W , mobility of the medium β , electroosmotic parameter m , and Darcy number Da are plotted for velocity distribution. Figure 2(a) shows the fluctuation in axial velocity f for various values of non-Newtonian fluid parameter $W = 0.0, 0.1, 0.3$. The velocity profile decreases at $\eta = 0$ and increases near the right wall of the channel as value of Weissenberg W increases. This suggests that non-Newtonian

Figure 2: Axial velocity f profile for (a). W (b). β (c). m (d). Da .

parameter have an influential impact on electroosmotic peristaltic motion. It also narrates that the velocity profile for viscous fluid ($W = 0$) is higher as compared to Williamson fluid velocity for current study. The effect of electroosmotic parameter β on the velocity profile is shown in Figure 2(b), it indicates that the axial velocity decreases at $\eta = 0$ considerably when the value of β is increased. Since, when $\beta = 0$, it vanishes electroosmotic effect throughout the channel. The effect of the electroosmotic parameter on the velocity profile is seen in Figure 2(c). By increasing the value of electroosmotic parameter m , strong effect on flow at the central region can be seen. Since the electroosmotic parameter defines the ratio of channel altitude to Debye length thickness λ_D . This means that as λ_D grows, reduces the EDL, and a huge amount of fluid flows. The amplitude of the velocity decreases at the right wall as the Da parameter is increased, while the opposite behavior is observed at $\eta = 0$ as shown in Figure 2(d). It's also worth noting that higher the Da value, the less porosity come to play implying absence of porous medium. A higher Da number results in

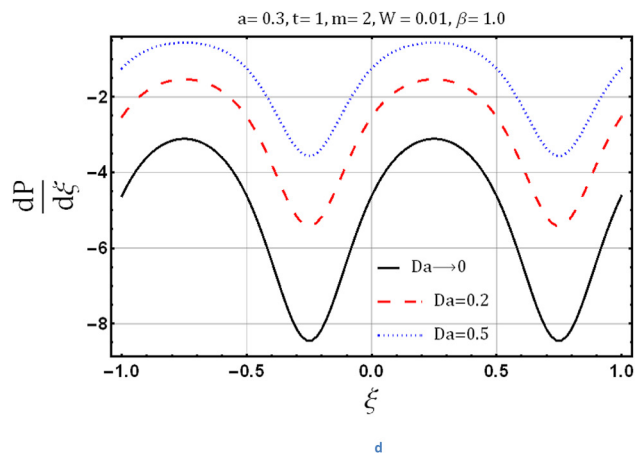
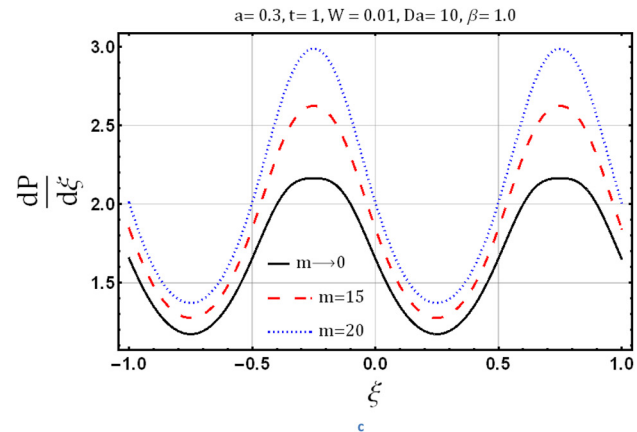
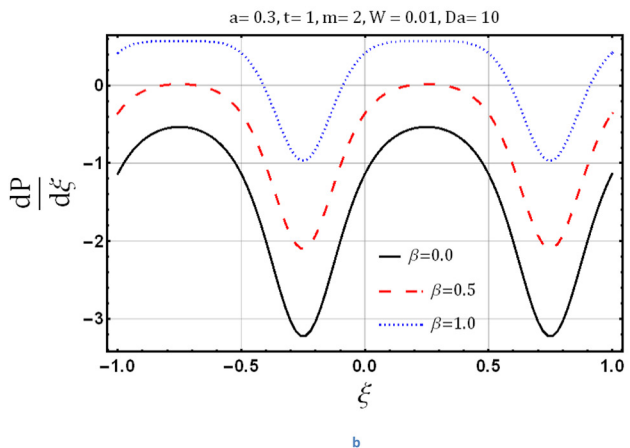
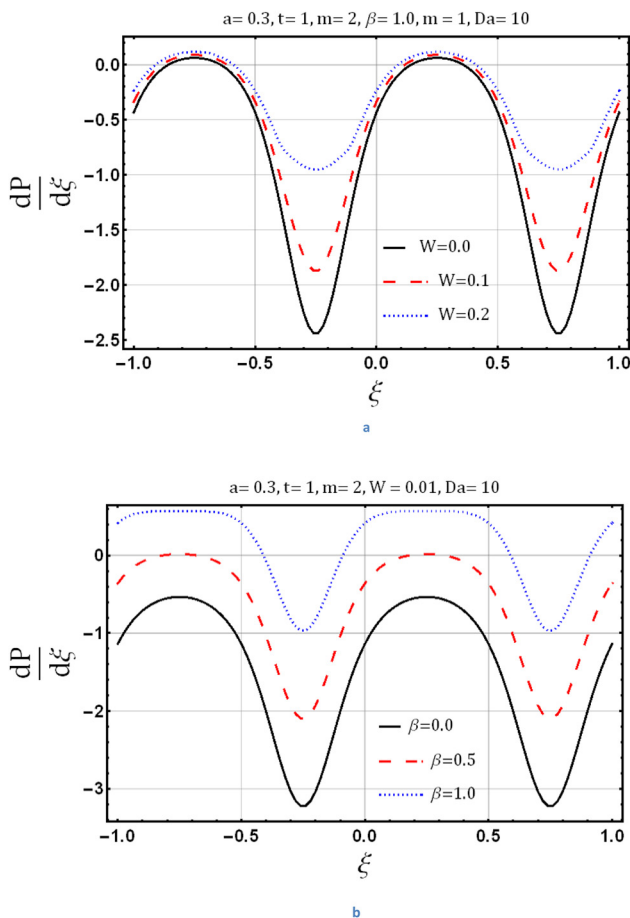


Figure 3: (continued)

larger pores, which increases the velocity and allows more fluid to pass through.

Table 1 is plotted to draw comparison of exact and numerical solution for electroosmotic and Darcy's porosity flow ($W = 0$). Good comparison can be seen for both cases. Table 2 is plotted to observe comparison between analytical and numerical solution for $\Psi''[h]$ in Williamson fluid flow ($W > 0$) in an electrohydrodynamic porous environment. Comparison is particularly drawn for fluid parameter W and modified Darcy parameter Da . For small values of W and Da good comparison in solution is observed. Table 3 is plotted to draw comparison of shear stress at wall for Darcy and modified Darcy case. It is observed that shear stress at wall is more for modified Darcy case.

4.2 Pumping characteristics

The peristaltic fluid movement is well recognized to be linked to mechanical pumping. Figure 3(a–d) depicts the pressure gradient distribution $dp/d\xi$ for the parameters

Figure 3: Pressure gradient $\frac{dp}{d\xi}$ profile for (a) W (b) β (c) m (d) Da .

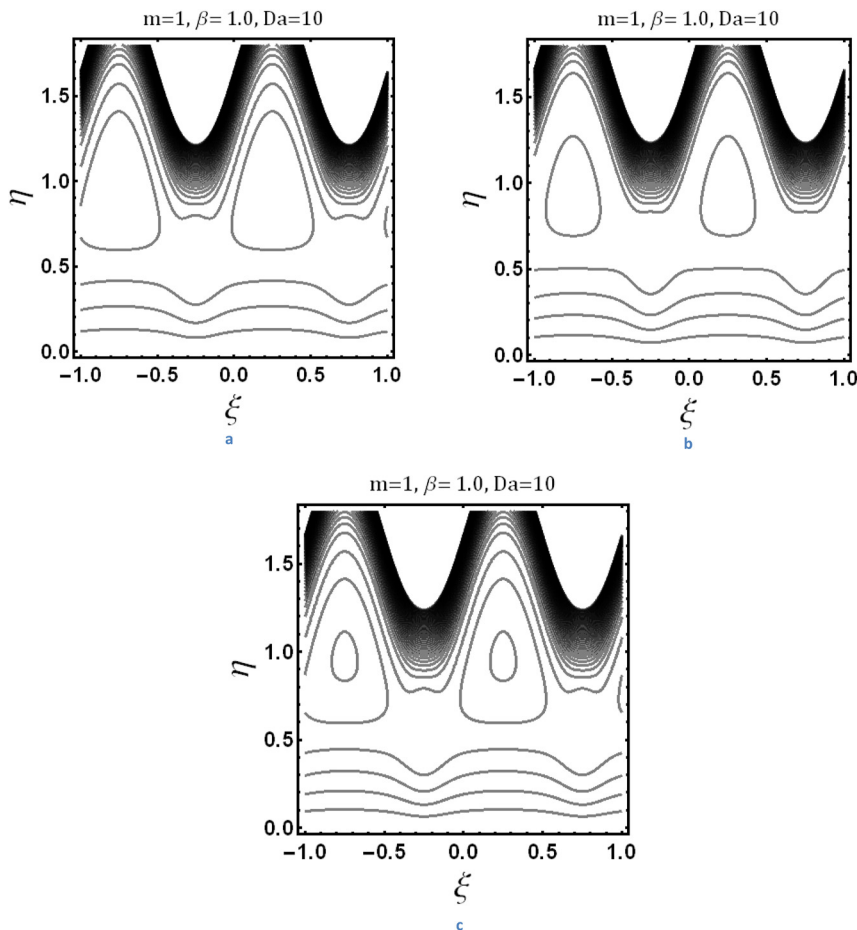


Figure 4: Streamline distribution for (a). $W = 0.00$ (b). $W = 0.01$ (c). $W = 0.02$.

Weissenberg number W , mobility of the medium β , electroosmotic parameter m and Darcy parameter Da . The behavior of W is analyzed in Figure 3(a). As values of W increases, the magnitude of the pressure gradient grows. W are inversely proportional to the channel width. As a result, the smaller the channel width, the more pressure is required to keep the flux flowing through it. Similarly, the value of the mobility of medium β increases, the pressure gradient arises, as illustrated in Figure 3(b) and the electroosmotic parameter m exhibits the same pattern as shown in Figure 3(c). In an electrically charged surface, EDL is present which opposes Williamson's fluid flow. Moreover, the electric double layer system can be used to regulate the pumping traits and the pumping process could be formalized by reducing and increasing the width of electric double layer. This feature is very helpful as surgeries require controlled flow. As the Darcy parameter Da grows, the pressure gradient increases, as seen in Figure 3(d). In comparison to a non-porous medium, a larger pressure gradient is required

to drive the fluid forward in the case of porous material. As a result, the fluid must be transported at a high-pressure gradient.

4.3 Trapping

Another interesting feature of peristaltic transport is trapping. The peristaltic wave pushes an internally rotating bolus of fluid forward through closed streamlines, causing trapping. Figures 4–7 are made to study the trapping phenomenon which is described by streamlines. Figure 4(a–c) depicts that the trapped bolus enlarges when the fluid properties shift from viscous fluid ($W = 0$) to Williamson fluid ($W > 0$). The streamline structure for various β values is shown in Figure 5 (a–c) As the value of β rises, the enclosed bolus size decreases. As m grows, the volume of the contained bolus increases, as seen in Figure 6(a–c). Since Williamson fluid's non-Newtonian nature, the number of trapped boluses reduces as m increases. The trapped

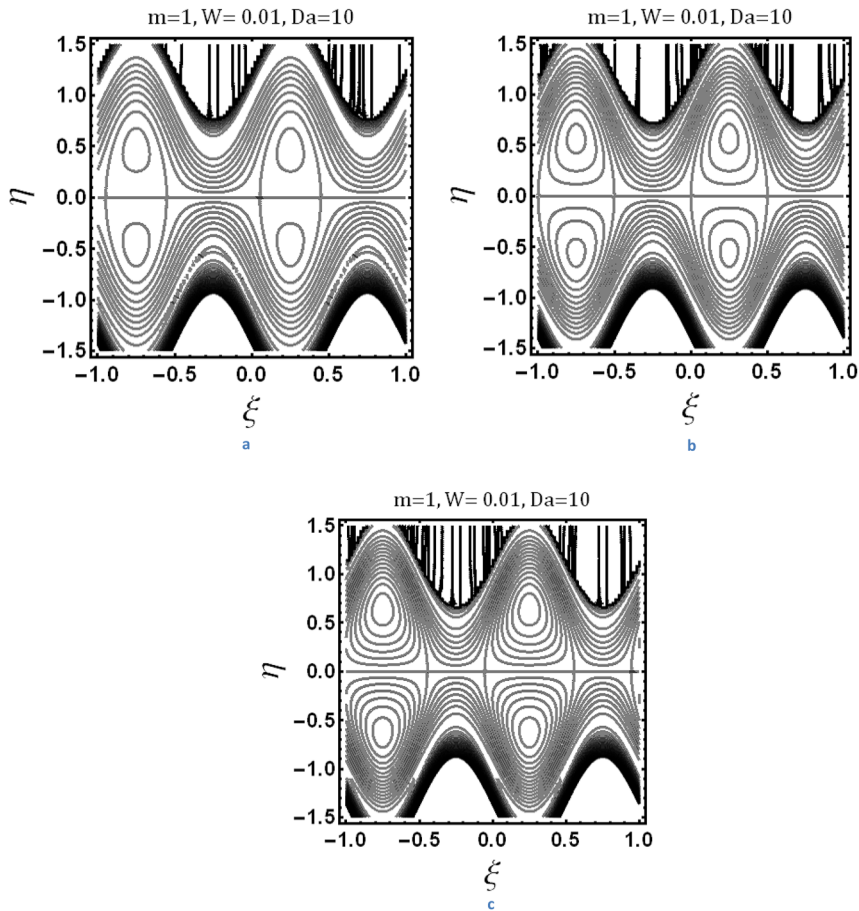


Figure 5: Streamline distribution for (a). $\beta = 1.5$ (b). $\beta = 2.0$ (c). $\beta = 3.0$.

bolus in EDL is seen to increase as the m increases. It also looks into how the trapped bolus in EDL reduces as the value of m falls. The effect of the Darcy parameter Da on

trapped bolus is shown in Figure 7(a–c). The size of the trapped bolus increases when the Darcy parameter Da is increased.

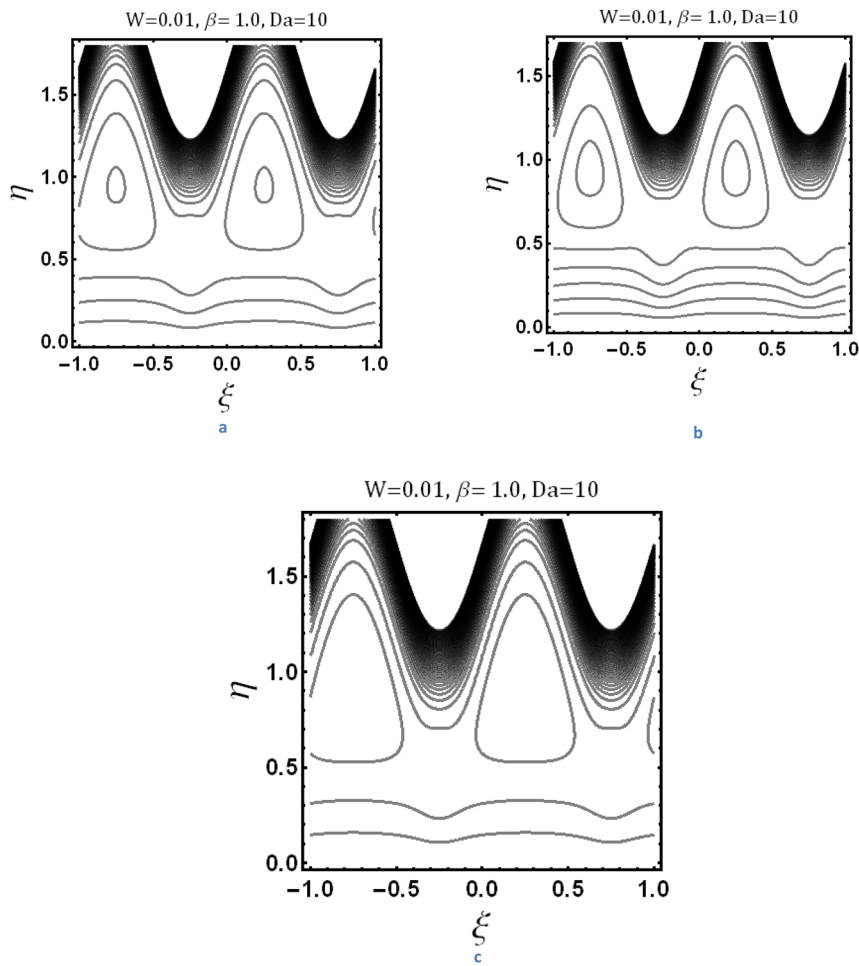


Figure 6: Streamline distribution for (a). $m = 5.0$ (b). $m = 5.2$ (c). $m = 5.5$.

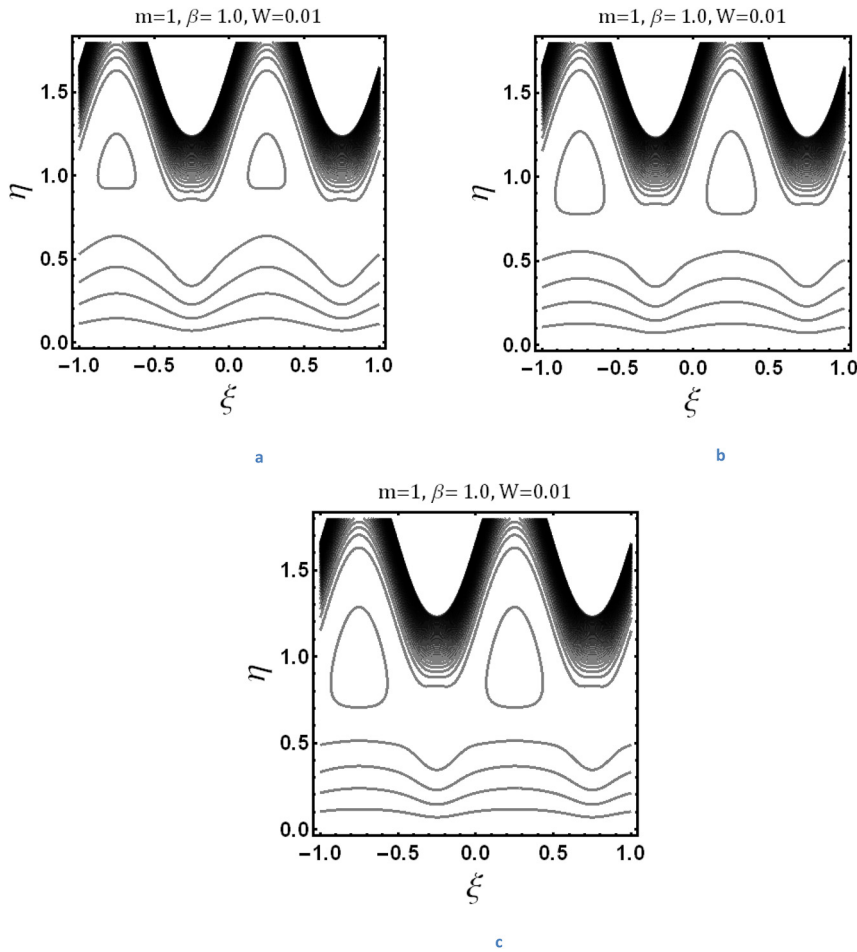


Figure 7: Streamline distribution for (a). $Da = 0.2$ (b). $Da = 0.5$ (c). $Da = 1.2$.

Table 1: Comparison of exact [6] and numerical solutions for varying electroosmotic velocity and Darcy's porosity where $W = 0, a = 0.3, x = 0.3, t = 1, C = 1, D = 1, m = 1.0$.

β	Da	$\Psi'' [h]$	
		Exact solution	Numerical solution
0	2	-0.700328	-0.700328
2		-0.855976	-0.855976
-2		-0.544681	-0.544681
-1	2	-0.622504	-0.622504
	5	-0.600606	-0.600606
	10	-0.593166	-0.593166

Table 2: Comparison of analytical and numerical solutions for $\Psi'' [h]$ where $a = 0.3, x = 0.3, F = Ce^{-Dt}, t = 1, C = 1, D = 1, m = 1.0, \beta = 1$.

W	Da	$\Psi'' [h]$	
		Analytical solution	Numerical solution
0	2	-0.778152	-0.778152
0.01		-0.780599	-0.7805632
0.02		-0.783047	-0.783181
0.01	0.5	-0.873345	-0.873397
	3	0.76956	-0.769591
	10	-0.753825	-0.753853

Table 3: Comparison of Shear stress at wall for darcy and modified Darcy case where, $\beta = 1, \alpha = 0.3, x = 0.3, t = 1$.

Da	W	m	$S_{\xi\eta} = \left(1 + W \frac{\partial \Psi^2}{\partial \eta^2}\right) \frac{\partial \Psi^2}{\partial \eta^2}$	$S_{\xi\eta} = \left(1 + W \frac{\partial \Psi^2}{\partial \eta^2}\right) \frac{\partial \Psi^2}{\partial \eta^2}$
			Darcy	Modified Darcy
1.1	0.03	1	-0.68273	-0.684535
1.5			-0.670457	-0.71711
02			-0.661764	-0.662664
201			-0.637181	-0.63259
200			-0.634629	-0.634636
500	0.01		-0.634458	-0.634461
0.2			-0.712437	-0.712622
			-0.973872	-0.978815
	0.1		-0.973872	-0.978815
	0.2		-0.914444	0.924378
0.2	0.1	1	-0.973872	-0.978815
		2	-1.32167	-1.33159
		3	-1.8649	-1.88126

5 Concluding remarks

This study explores the analytical and numerical results for Darcy's resistance and electrokinetic on Williamson fluid flow using lubrication and Debye-Huckel approaches. The perturbation technique is used to obtain analytical solutions. Numerical simulation by using built in MATHEMATICA coding has also been used to validate the perturbation solution. The following are some important conclusions:

- Modified Darcy law usage for porosity effect in electroosmotic peristaltic channel is more authentic.
- The axial velocity increases at ($\eta = 0$ i.e. centre) and decreases near the right wall of the channel as the value of W, β, m increases.
- Shear stress is more modified Darcy's case than Darcy at channel wall.
- The axial velocity decreases near the right wall of the channel as the value of Darcy number Da increases.
- Pressure gradient grows with increasing value of Weissenberg number W , mobility of medium β , electroosmotic parameter m , Darcy number Da .
- In comparison to a non-porous medium, a larger pressure gradient is required to drive the fluid forward in the case of porous material.
- The trapped bolus decreases as value of W and β grows. The bolus size increases as value of m and Da increases.

- Velocity and pressure gradient are smaller and larger in magnitude respectively, when comparison is drawn for Williamson and viscous fluid flowing in porous matrix governed by modified Darcy's law.

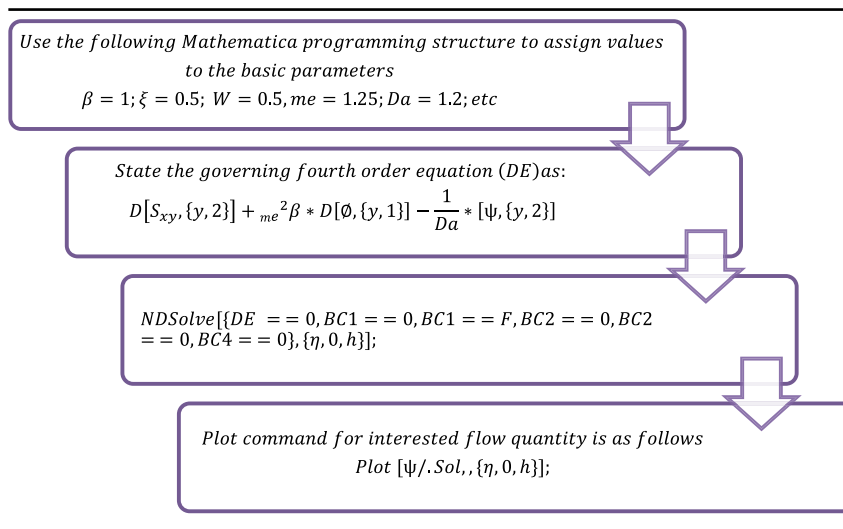
As a result, the impacts of non-Newtonian fluid behavior, outer electric field, electric double layer thicknesses, and varied flow pattern geometries cannot be neglected while analyzing electroosmotic modulating peristaltic flow in microchannels for manufacturing bio-microfluidic equipment. This model can be used in a variety of biochemical flows that are governed by electroosmosis and fluid thermal properties. A possible extension of current study is to investigate the effect of incorporating nanoparticles into Williamson fluid flow, while considering the influence of Darcy's resistance and electrokinetics to explore the potential applications of hybrid nanofluids.

Author contributions: All the authors have accepted responsibility for the entire content of this submitted manuscript and approved submission.

Research funding: None declared.

Conflict of interest statement: The authors declare that they have no competing interests.

Appendix Numerical solution

Table 4: Flow chart of numerical scheme.

Analytical solution

Zero order solution $O(W)^0$

$$\psi_0 = \frac{-e^{\sqrt{Da}y}A_1 - e^{-\sqrt{Da}y}A_2}{Da} + A_3 + yA_4 + \frac{L2\text{Sinh}[m\eta]}{m^2(Da - m^2)}, \quad (41)$$

$$\frac{dp_0}{d\xi} = \frac{e^{\sqrt{Da}y}A_1}{Da\sqrt{Da}} + \frac{e^{-\sqrt{Da}y}A_2}{\sqrt{Da}} + e^{-\sqrt{Da}\eta} \sqrt{Da} \left(-e^{2\sqrt{L3}y}A_1 + A_2 \right) + A_4 + L1\text{Cosh}[m\eta] + \frac{L2m\text{Cosh}[m\eta]}{Da - m^2} + \frac{L2\text{Cosh}[m\eta]}{Dam - m^3}, \quad (42)$$

First order solution $O(W)^1$

$$\begin{aligned} \psi_1 = & ((e^{2\sqrt{L3}y}(-1 - DaL3 + 2D^2L3^2)(-L3 + m^2)^2(1 - 2DaL3 + Da^2L3^2 - 2Dam^2 \\ & - 2Da^2L3m^2Da^2m^4)(1 - 5Dam^2 + 4D^2m^4)A_1^2)/(4(-1 + \sqrt{Da}\sqrt{L3})(1 + \sqrt{Da}\sqrt{L3}) \\ & \times (e^{\frac{(1+4\sqrt{Da}\sqrt{L3})y}{\sqrt{Da}}}(-Da(1+m)(-L3+m^2)(1-2DaL3+Da^2L3^2-2Dam^2-2Da^2L3m^2+Da^2m^4) \\ & + \frac{1}{\sqrt{L3+m}}e^{-\frac{(1+4\sqrt{Da}\sqrt{L3})y}{\sqrt{Da}}} + \frac{(1+5\sqrt{Da}\sqrt{L3})y}{\sqrt{Da}}(DaL3A_1 - Da^2L3^2A_1 + 2\sqrt{L3}mA_1 - Da\sqrt{L3}mA_1 - DaL3^{3/2}mA_1 + 2Da^2m^6A_2 \\ & - 12Da^3L3m^6A_2 - 4Da^3\sqrt{L3}m^7A_2)) + (e^{\frac{(1+4\sqrt{Da}\sqrt{L3})y}{\sqrt{Da}}}(Da(-1+m)m(-L3+m^2)(1-2DaL3+Da^2L3^2-2Dm^2-2Da^2L3m^2 \\ & + Da^2m^4) + Da^3\sqrt{Dam^6}A_2 + 12Da^3L3^{3/2}m^6A_2 + 2Da^2m^7A_2 - 12Da^3Dam^7A_2 + 4Da^3\sqrt{Dam^8}A_2)) \\ & - 192Da^6L2Da^{7/2}m^9A_2 + 16Da^4L2Dam^{10}A_2 - 80Da^5L2Da^2m^{10}A_2 \\ & + 64Da^6L2Da^3m^{10}A_2)(\text{Cosh}[m\eta](\text{Cosh}[m\eta] - \text{Sinh}[m\eta])^2(\text{Cosh}[m\eta] + \text{Sinh}[m\eta])) \\ & - 2Da^2e^{\frac{(1+3Da)\eta}{\sqrt{Da}}}m^6A_2 + 12Da^3e^{\frac{(1+3Da)\eta}{\sqrt{Da}}}Dam^6A_2 - 4Da^3e^{\frac{(1+3\sqrt{Da}\sqrt{L3})y}{\sqrt{Da}}}\sqrt{Dam^7}A_2(-1 + \sqrt{Da}\sqrt{Da} + \sqrt{Dam})(1 + \sqrt{Da}\sqrt{L3} \\ & + \sqrt{Dam})(-1 + 2\sqrt{Dam})(1 + 2\sqrt{Dam})(4(-1 + Da)(1 + Da)(-1 + 2\sqrt{Da}\sqrt{Da})(1 + 2\sqrt{Da}\sqrt{Da})\sqrt{Da} \\ & \times (\sqrt{Da} - m)^2m(\sqrt{Da} + m)^2(-1 + Da - \sqrt{Dam})(1 + Da - \sqrt{Dam})(-1 + \sqrt{Dam}) \\ & \times (1 + \sqrt{Dam})(-1 + Da + \sqrt{Dam})(-1 + 2\sqrt{Dam})(1 + 2\sqrt{Dam})) + Da e^{\frac{\eta}{\sqrt{Da}}}B_1 + Da e^{-\frac{\eta}{\sqrt{Da}}}B_2 + B_3 + \eta B_4 \end{aligned}$$

$$\begin{aligned}
\frac{dp_1}{d\xi} = & \frac{A_2 e^{-\sqrt{Da}\eta}}{Da} + 2A_1 e^{\sqrt{Da}\eta} + \frac{e^{-\sqrt{L_3}y}(-A_2 + A_1 e^{2\sqrt{Da}\eta})}{\sqrt{L_3}} + 2e^{-\sqrt{Da}\eta}(-A_2 + A_1 e^{2\sqrt{Da}\eta})\sqrt{Da} + \frac{A_2 e^{-\sqrt{L_3}y} L_2 m \text{Cosh}[m\eta]}{Da - m^2} \\
& + \frac{L_2 \text{Cosh}[m\eta]}{Dam - m^3} + \frac{L_2 \text{Sinh}[m\eta]}{Da - m^2} + \frac{A_4 L_2 \text{Sinh}[m\eta]}{Da - m^2} - \frac{1}{8Da} (8B_4 - 8B_2 \sqrt{Da} e^{-\frac{\eta}{\sqrt{Da}}} + 8B_1 \sqrt{Da} e^{\frac{\eta}{\sqrt{Da}}}) \\
& - \frac{4A_1^2 e^{2\sqrt{Da}\eta} (1 + 2Da)}{\sqrt{L_3}(-1 + 4Da)} - \frac{8A_1 Dae^{\sqrt{Da}\eta} (1 + \sqrt{Da} + Da^{3/2})}{L_3(-1 + Da)} \\
& \times \frac{2A_2 e^{-2\sqrt{Da}\eta} (1 + 4\sqrt{Da})(-A_2 \sqrt{Da} + 2Da^2 Da (8e^{\sqrt{L_3}y}(-1 + 2\sqrt{Da}) + A_2 Da^{3/2}) - Da(e^{\sqrt{Da}\eta}(-4 + 8\sqrt{Da}) + A_2 Da^{3/2}))}{\sqrt{Da} Da^{3/2} (1 - 5Da L_3 + 4Da^2 Da^2)} \\
& + 8(A_4 + A_1 A_2 (2 - 4Da))y + \frac{4L_2^2 (-1 + 2Dam^2)\eta}{(Da - m^2)^2} - \frac{L_2^2 (1 + 2Dam^2) \text{Cosh}[2m\eta]}{m(Da - m^2)^2 (-1 + 4Dam^2)} \quad (43)
\end{aligned}$$

$A_1, A_2, A_3, A_4, B_1, B_2, B_3, B_4$, are constants evaluated from Mathematica software.

References

- [1] E. C. Childs and E. Tzimas, "Darcy's law at small potential gradient," *J. Soil Sci.*, vol. 22, pp. 319–327, 1971.
- [2] S. Whitaker, "Flow in porous media I: a theoretical derivation of Darcy's law," *Transp. Porous Media*, vol. 1, pp. 3–25, 1986.
- [3] M. K. Hubbert, "Darcy's law and the field Equations of the flow of undergrounds fluids," *Pet. Trans. AIME*, vol. 207, pp. 222–239, 1956.
- [4] V. M. Starov and V. G. Zhdanov, "Effective viscosity and permeability of porous medium," *Colloides Surf., A*, vol. 192, pp. 363–375, 2001.
- [5] D. R. Graham and J. J. L. Higdon, "Oscillatory forcing of flow through porous media. Part 1. Steady flow," *J. Fluid Mech.*, vol. 465, pp. 213–235, 2002.
- [6] T. Hayat, Q. Hussain, and N. Ali, "Influence of partial slip on the peristaltic flow in a porous medium," *Phys. A*, vol. 387, pp. 3399–3409, 2008.
- [7] K. Ramesh, "Influence of heat and mass transfer on peristaltic flow of a couple stress fluid through porous medium in the presence of inclined magnetic field in an inclined asymmetric channel," *J. Mol. Liq.*, vol. 219, pp. 256–271, 2016.
- [8] T. Sajid, M. Sagheer, S. Hussain, and M. Bilal, "Darcy-Forchheimer flow of Maxwell Nanofluid flow with nonlinear thermal radiation and activation energy," *AIP Adv.*, vol. 8, 2018, Art. no. 035102.
- [9] M. Bilal and M. Ramzan, "Hall current effect on unsteady rotational flow of carbon nanotubes with dust particles and nonlinear thermal radiation in Darcy-Forchheimer porous media," *J. Therm. Anal. Calorim.*, vol. 138, 2019. <https://doi.org/10.1007/s10973-019-08324-3>.
- [10] M. Ramzan, M. Bilal, and C. J. Dong, "Numerical simulation of magnetohydrodynamic radiative flow of casson nanofluid with chemical reaction past a porous media," *J. Comput. Theor. Nanosci.*, vol. 14, pp. 5788–5796, 2017.
- [11] D. C. Lu, M. Ramzan, M. Bilal, C. J. Dong, and U. Farooq, "Upshot of chemical species and nonlinear thermal radiation on oldroyd-B nanofluid flow past a Bi-directional stretched surface with heat generation/absorption in a porous media," *Commun. Theor. Phys.*, vol. 70, 2018, Art. no. 071.
- [12] S. Gisinger, A. Dornbrack, and J. Schrottelle, "A modified Darcy's law," *J. Theor. Comput. Fluid Dynam.*, vol. 29, pp. 343–347, 2015.
- [13] C. Vasudev, U. R. Rao, M. S. Reddy, and G. P. Rao, "Peristaltic pumping of Williamson fluid through a porous medium in a horizontal channel with heat transfer," *A. m. J. Sci. Ind. Res.*, vol. 1, pp. 656–666, 2010.
- [14] N. A. Khan, S. Khan, and A. Ara, "Flow of micropolar fluid over an off centered rotating disk with modified Darcy's law," *Propul. Power Res.*, vol. 6, pp. 285–295, 2017.
- [15] K. K. Imomnazarov, "Modified Darcy's law for conducting porous media," *Math. Comput. Model.*, vol. 40, pp. 5–10, 2004.
- [16] S. Wada, N. Nishiyama, and S. Nishida, "Modified Darcy's law for Newtonian fluids," *Bulletin JSME*, vol. 28, pp. 3031–3037, 1985.
- [17] T. Hayat, M. Khan, and S. Asghar, "On the MHD flow of fractional generalized Burgers' fluid with modified Darcy's law," *Acta Mech. Sin.*, vol. 23, pp. 257–261, 2007.
- [18] T. Hayat, S. Nawaz, and A. Alsaedi, "Entropy generation and endoscopic effects on peristalsis with modified Darcy's law," *Physica A: Statistical Mech. and its app.*, vol. 536, 2017, Art. no. 120846.
- [19] N. Imran, M. Jawad, M. Sohail, and I. Tlili, "Utilization of modified Darcy's law in peristalsis with a compliant channel: applications to thermal Science," *J. Mater. Res. Technol.*, vol. 9, pp. 5619–5629, 2020.
- [20] Forchheimer, "Wasserbewegung durch Boden," *Z. Ver. Deutsch. Ing.*, vol. 45, pp. 1782–1788, 1901.
- [21] S. Noreen and A. Qurat, "Entropy generation analysis on electroosmotic flow in non-Darcy porous medium via peristaltic pumping," *J. Therm. Anal. Calorim.*, vol. 137, pp. 1991–2006, 2019.
- [22] N. T. M. Eldabe, M. Abouzeid, M. A. A. Mohamed and M. M. Abd-Elmoneim, "MHD peristaltic flow of non-Newtonian power-law nanofluid through a non-Darcy porous medium inside a non-uniform inclined channel," *Arch. Appl. Mech.*, vol. 91, pp. 1067–1077, 2021.
- [23] A. Gupta, D. Coelho, and P. M. Adler, "Universal electro-osmosis formulae for porous media," *J. Colloid Interface Sci.*, vol. 319, pp. 549–554, 2008.
- [24] S. Chen, X. He, V. Bertola, and M. Wang, "Electroosmosis of non-Newtonian fluid in porous media using Lattice Poisson-Boltzmann method," *J. Colloid Interface Sci.*, vol. 436, pp. 186–193, 2014.

- [25] W. R. Bowen and R. A. Clark, "Electro-osmosis at micro-porous membranes and the determination of zeta-potential," *J. Colloid Interface Sci.*, vol. 97, pp. 401–409, 1984.
- [26] P. Gravesen, J. Branebjerg, and O. S. Jensen, "Microfluidics a review," *J. Micromech. Microeng.*, vol. 3, p. 168, 1993.
- [27] S. C. R. Dennis and F. T. Smith, "Steady flow through channel with a symmetrical contraction in the form of step," *Proc. R. Soc. London.*, vol. 372, pp. 393–414, 1980.
- [28] T. P. Chiang and W. H. Sheu Tony, "Bifurcation of flow through plane symmetric channel contraction," *J. Fluids Eng.*, vol. 124, pp. 444–451, 2002.
- [29] T. Hawa and Z. Rusak, *The Dynamics of a Laminar Flow in a Symmetric Channel with a Sudden Expansion*, Cambridge University Press, 2001, pp. 283–320.
- [30] T. W. Latham, "Fluid motion in peristaltic pump," M.S. thesis, Cambridge, MA, M.I.T, 1966.
- [31] E. F. Elshehawey, N. T. Eldabe, E. M. Elghazy, and A. Ebaid, "Peristaltic transport in an asymmetric channel through a porous medium," *Appl. Comput. Math.*, vol. 182, pp. 140–150, 2006.
- [32] G. R. Machireddy and V. R. Kattamreddy, "Impact of velocity slip and joule heating on MHD peristaltic flow through porous medium with chemical reactions," *J. Nigerian Math. Soc.*, vol. 35, pp. 227–244, 2016.
- [33] A. Bertuzzi, S. Salinari, R. Mancinelli, and M. Pescatori, "Peristaltic transport of a solid bolus," *J. Biomech.*, vol. 16, pp. 459–464, 1983.
- [34] J. C. Misra and S. K. Pandey, "Peristaltic transport of blood in small vessels: study of mathematical model," *Compute. Math. Appl.*, vol. 43, pp. 1183–1193, 2002.
- [35] M. Mishra and A. R. Rao, "Peristaltic transport of a Newtonian fluid in an asymmetric channel," *Z. Angew. Math. Phys.*, vol. 54, pp. 532–550, 2003.
- [36] S. Chakarborty, "Augmentation of peristaltic micro flows through electroosmotic mechanisms," *J. Phys.*, vol. 39, pp. 5256–5363, 2006.
- [37] K. Vajravelu, G. Radhkrishnamacharva, and V. Radhkrishnamurthy, "Peristaltic flow and heat transfer in a vertical porous annulus with long wave approximation," *Int. J. Non-Linear Mech.*, vol. 42, pp. 754–759, 2007.
- [38] S. Srinivas and M. Kothandapani, "The influence of heat and mass transfer on MHD peristaltic flow through a porous space with compliant walls," *Appl. Math. Compute.*, vol. 212, pp. 197–208, 2009.
- [39] D. Tripathi, "Peristaltic transport of a viscoelastic fluid in a channel," *Acta Astronaut.*, vol. 68, pp. 1379–1385, 2011.
- [40] M. M. Bhatti, S. M. Sait, and R. Ellahi, "Magnetic nanoparticles for drug delivery through tapered stenosed artery with blood based non-Newtonian fluid," *Pharmaceuticals*, vol. 15, p. 1352, 2022.
- [41] M. M. Bhatti and S. I. Abdelsalam, "Scientific breakdown of a ferromagnetic nanofluid in hemodynamics: enhanced therapeutic approach," *Math. Model. Nat. Phenom.*, vol. 17, no. 25, 2022. <https://doi.org/10.1051/mmnp/2022045>.
- [42] S. Akram, S. Nadeem, and M. Hanif, "Numerical and analytical treatment on peristaltic flow of Williamson fluid in the occurrence of induced magnetic field," *J. Magn. Magn Mater.*, vol. 346, pp. 142–151, 2013.
- [43] M. Khan and A. Hamid, "Influence of non-linear thermal radiation on 2D unsteady flow of a Williamson fluid with heat source/sink," *Results Phys.*, vol. 7, pp. 3968–3975, 2017.
- [44] A. Hamid, Hashim, and M. Khan, "Numerical simulation for heat transfer performance in unsteady flow of Williamson fluid driven by a wedge-geometry," *Results Phys.*, vol. 9, pp. 479–485, 2018.
- [45] A. H. Hashim and M. Khan, "Unsteady mixed convective flow of Williamson nanofluid with heat transfer in the presence of variable thermal conductivity and magnetic field," *J. Mol. Liq.*, vol. 260, pp. 436–446, 2018.